The 14th International Topical Meeting on Nuclear Reactor Thermalhydraulics, NURETH-14
Toronto, Ontario, Canada, September 25-30, 2011

NURETH14-387

DROPLET ENTRAINMENT AND DEPOSITION RATE MODELS FOR DETERMINATION OF BOILING TRANSITION IN BWR FUEL ASSEMBLY

B. Hizoum, P. Saha, J. G. M. Andersen and K. Whitlow
GE Hitachi Nuclear Energy, Wilmington, NC, USA

Abstract

Droplet entrainment and deposition rates are of vital importance for mechanistic determination of critical power and location of boiling transition in a BWR fuel assembly. Data from high-pressure, high-temperature steam-water adiabatic experiments conducted in very tall test sections are used to develop a combination of equilibrium entrainment-deposition rate. Application of this combination to the heated tests conducted in a shorter test section of typical height of a BWR fuel assembly shows that correct split of total liquid in form of the film and droplets at the onset of annular-mist flow regime is also important to obtain good prediction of film flow rates/entrainment fraction. The improved model is then applied to simulate critical power tests in annulus and rod bundles.

Introduction

GE Hitachi Nuclear Energy (GEH) has developed a detailed subchannel analysis code COBRAG [1] with the main objective of predicting the critical power, the bundle pressure drop and the void distribution in BWR fuel bundles. The two-phase flow is described by conservation equations derived from a two-fluid (e.g. liquid and vapor), multi-field (e.g. continuous, dispersed and multifilm) model. This model, which allows liquid films on different surfaces within a subchannel to have their own set of conservation equations, proves to be crucial in predicting dryout or onset of boiling transition (BT) that may occur on rods next to unheated surfaces (e.g., channel wall and water rod). The conservation equations are then coupled with other physical models or constitutive relations for the wall and interfacial shear, interfacial heat transfer, liquid entrainment and deposition rates, inter-subchannel mixing, and void drift for closure.

Close scrutiny of COBRAG predictions [1] for entrainment fraction (defined by the mass flow rate of entrained liquid droplets in the continuous vapor phase divided by the total mass flow rate of liquid) for simple geometry experiments conducted at Risø [2] showed a need for further improvement of the entrainment and deposition rate models. Several models and correlations for droplet entrainment and deposition rates were examined, and finally a combination of separate entrainment and deposition rate models was selected based on high-pressure, high-temperature steam-water adiabatic experiments conducted in very tall test sections in round tube and annulus geometry [2]. Application of this combination of equilibrium entrainment/deposition rates to the heated tests conducted in a shorter test section of typical height of a BWR fuel assembly shows that correct split of total liquid in form of the film and droplets at the onset of annular-mist flow regime is also important to obtain good prediction of film flow rates/entrainment fraction.

Finally the improved model was used to predict critical power in annulus and rod bundle geometries.

1. Boiling transition (BT) in BWR condition

It is recognized [3] that the boiling transition (BT), which occurs at relatively higher qualities in a BWR, is primarily due to a dryout of liquid film on the heated surface. This phenomenon is associated with two-phase annular and annular-mist flow regimes that have been studied extensively [4, 5]. Once the liquid film vanishes or becomes extremely thin, the convective heat transfer at the heated surface deteriorates and the surface temperature starts to increase, normally with some oscillation [3].

A simple film dryout model [3] is shown in Figure 1.

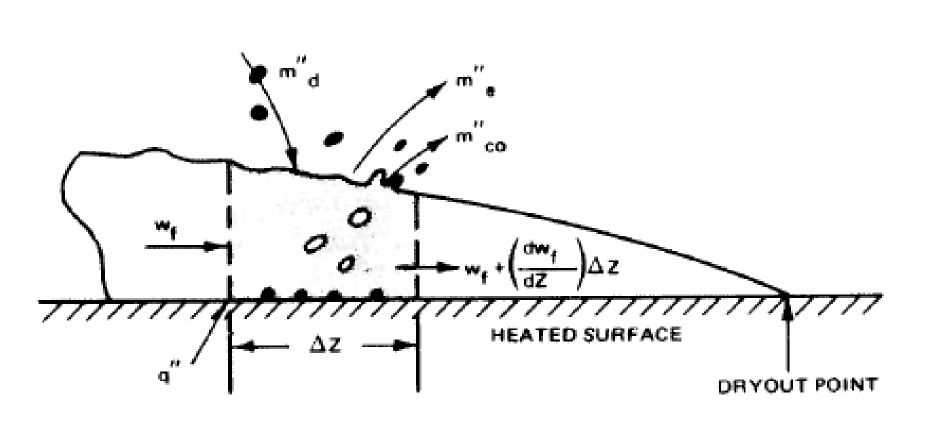

Figure 1 A simple film dryout model for determination of boiling transition (BT)

The liquid film at the heated surface is depleted by liquid evaporation due to heat addition, liquid entrainment ($m_e^{''}$) due to shearing off liquid from the top of wavy liquid film by the turbulent high-velocity vapor, and possible liquid carry over ($m_{co}^{''}$) by any vapor bubble that may burst through the liquid film. On the other hand, deposition of liquid droplets ($m_d^{''}$) from the vapor core replenishes the liquid film on the heated surface. In the pre-dryout annular-mist region, both liquid and vapor are at saturated condition. The conservation of mass principle applied to a saturated liquid film implies that at steady state, the axial gradient of liquid film mass flow rate (w_f) can be expressed as [3]

$$\frac{dw_f}{dz} = \xi_h \left(m_d^{''} - \frac{q^{''}}{h_{fg}} - m_e^{''} - m_{co}^{''} \right) \quad (1)$$

where ξ_h is the heated perimeter (m), $m_d^{''}$ is the droplet deposition rate per unit area (kg/m^2-s), $q^{''}$ is the wall heat flux (J/m^2-s), h_{fg} is the latent heat of vaporization (J/kg), $m_e^{''}$ is the liquid entrainment rate per unit area (kg/m^2-s), and $m_{co}^{''}$ is the liquid carry over rate per unit area (kg/m^2-s).

Separate experimental determination of the liquid carry over term ($m_{co}^{"}$) is almost impossible. Therefore, effect of this carry over term, which is usually small compared to the other terms, is included in the entrainment term ($m_e^{"}$) in this paper. Equation (1) thus becomes

$$\frac{dw_f}{dz} = \xi_h \left(m_d^{"} - \frac{q^{"}}{h_{fg}} - m_e^{"} \right) \tag{2}$$

For a given heat flux and system pressure, determination of the liquid evaporation term ($q^{"} / h_{fg}$) is rather straightforward. Therefore, the liquid entrainment and deposition rates as well as the initial film flow rate at the transition to annular flow are the crucial parameters for determination of the dryout or BT point where the liquid film flow rate (w_f) becomes zero or near zero. In a rod bundle geometry, there are additional effects due to cross-flow and spacers, which influence the downstream behaviour of the liquid film, and the entrainment and deposition process.

1.1 Liquid entrainment rate

Direct measurement of droplet entrainment rate is very difficult since droplet entrainment is a complex phenomenon and it coexists with droplet deposition. However, in the hydrodynamic equilibrium state sufficiently downstream of gas-liquid mixing section where the liquid film flow rate does not change with axial distance, i.e., dw_f /dz approaches zero, the droplet entrainment and deposition rates in adiabatic ($q^{"}$ = 0) two-phase annular flow regime become equal as per Equation (2).

Early experimental studies [2, 4, 5] of annular two-phase flow focused on the extraction of the liquid film at the wall and thus provided data on the liquid film flow rate (w_f) and the total liquid entrainment fraction, E, defined by

$$E = \frac{w_d}{w_{liq}} = \frac{w_{liq} - w_f}{w_{liq}} \tag{3}$$

where w_{liq} is the total liquid flow rate in the film and in droplet form and w_d is the liquid flow rate only in the droplet form. Later, a second extraction station downstream of the first extraction station was added to directly determine the droplet deposition rate [5, 6]. Note that the data for the deposition rate obtained from the "double film extraction" method [5, 6] may be used to develop models or correlations for both the equilibrium deposition and entrainment rates. However, the physical basis of the correlations should be different since the mechanisms of droplet entrainment and droplet deposition are very different.

It is generally accepted that liquid droplets are sheared off from the top of disturbance wave in the liquid film by the action of vapor or gas flow in the core. A pictorial view of the mechanism of droplet entrainment [7] from the upward liquid film at the wall is shown in Figure 2. Thus many researchers [2, 8, 9] used a force balance between the interfacial shear stress and surface tension at the gas-liquid interface to form a governing non-dimensional parameter for the mechanism of entrainment, and then developed the theoretical models or correlations for the liquid entrainment rate, $m_e^{''}$.

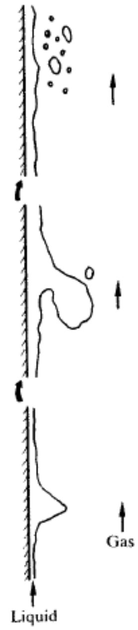

Figure 2 Mechanism of droplet entrainment from upward liquid film at the wall

1.2 Droplet deposition rate

The droplet deposition rate is usually assumed as a mass transfer process normal to the main flow direction. Therefore, almost all droplet deposition rate models start with the form

$$m_d^{''} = k_d C \qquad (4)$$

where k_d is the droplet mass transfer or deposition coefficient (m/s) and C is the droplet concentration (kg/m^3) in the vapor core.

Early work [10] on droplet deposition rate simply correlated the deposition coefficient k_d in terms of surface tension σ which is only a function of pressure for saturated steam-water system. In more recent work [11, 12, 9, 13], a non-dimensional form of droplet deposition coefficient ($k_d \sqrt{\rho_g D / \sigma}$) is correlated in terms of droplet concentration C and other fluid properties. Sugawara [8], on the other hand, invoked the similarity of heat and mass transfer in turbulent flow to correlate k_d in terms of vapor velocity u_g, vapor Reynolds number Re_g, droplet concentration C, vapor density ρ_g, and vapor Schmidt number Sc which is eventually set equal to vapor Prandtl number Pr_g assuming Lewis number to be unity.

Effect of various combinations of entrainment and deposition rate models has been studied through COBRAG for the Risø test data [2] obtained for liquid film flow rate and entrainment fractions in round tubes and annulus. The results are discussed in the following section.

2. Comparison of COBRAG Prediction with Risø Test Data

Würtz [2] conducted high pressure (30 to 90 bar) adiabatic steam-water flow experiments in vertical round tubes (10 and 20 mm I. D.) and annulus (17 mm I. D./26 mm O. D.) with long lengths (9 m and 8 m, respectively). Two-phase mixture with known flow rates of saturated water and steam was introduced at the test section inlet. The flow regime at the test section exit was annular or annular-mist, and the liquid film at the wall was extracted at the exit and the liquid entrainment fraction was thus determined. Because of the large length-to-diameter ratio, L/D_h, shown in Table 1, a near equilibrium condition was reached at the test section exit in terms of liquid film flow rate, and thus liquid entrainment and droplet deposition rates. Other test parameters are also shown in Table 1. Pressure drop was also measured during these tests and the COBRAG pressure gradients at the exit are compared to the measured data. This adds confidence to the wall and interfacial shear models used in COBRAG.

Table 1. Risø Adiabatic Test Conditions

	Series 200	**Series 600**	**Series 500**
Test Section Diameter (mm)	10 (Round Tube)	20 (Round Tube)	17I.D./26O.D. (Annulus); D_h = 9 mm
Length (m)	9	9	8
L/D_h	900	450	889
Pressure (bar)	30 – 90	70	30 – 90
Mass flux (kg/m^2-s)	500 – 3000	500 – 2000	400 – 2000
Exit vapor quality (-)	0.08 – 0.6	0.2 – 0.7	0.15 – 0.6

Würtz [2] also conducted experiments in heated or diabatic test sections of various configurations. The most appropriate tests for COBRAG simulations are Runs 106, 114-116 and 126 performed at 70 bar in a 3.5 long annulus with a 17 mm diameter heated inner rod in a 26 mm diameter unheated outer tube. Liquid films were extracted from both the inner and outer surfaces of the annulus at the exit, and thus the entrainment fraction at the exit was determined.

2.1 Comparison with Risø Adiabatic Tests

COBRAG simulation of Risø adiabatic tests is very straightforward. Test values of saturated water and steam flows are supplied as the inlet boundary condition and system pressure is provided as the exit boundary condition. Various combinations of entrainment and deposition rate models/correlations were attempted and the best combination was selected and ‘frozen’. Figures 3 to 5 show the comparison of COBRAG predictions (with the selected combination) for exit entrainment fraction and exit pressure gradient with the test data for both the round tubes (10 and 20 mm diameter) and the annulus.

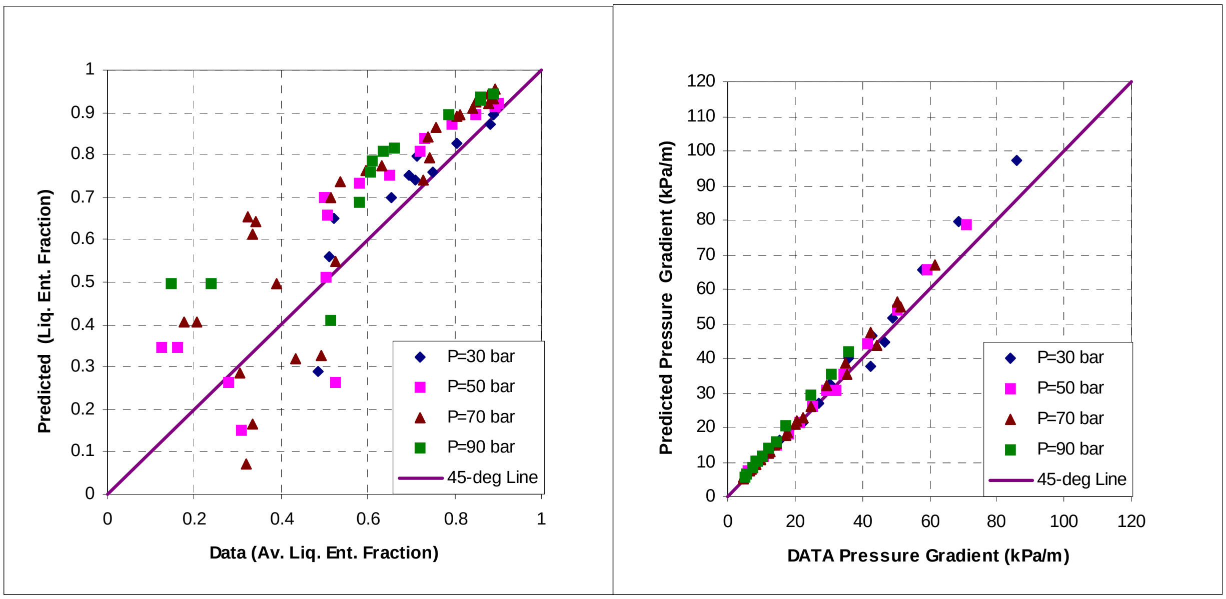

Figure 3 Comparison of COBRAG Prediction with Risø 200 Series Data in 10 mm diameter Round Tube

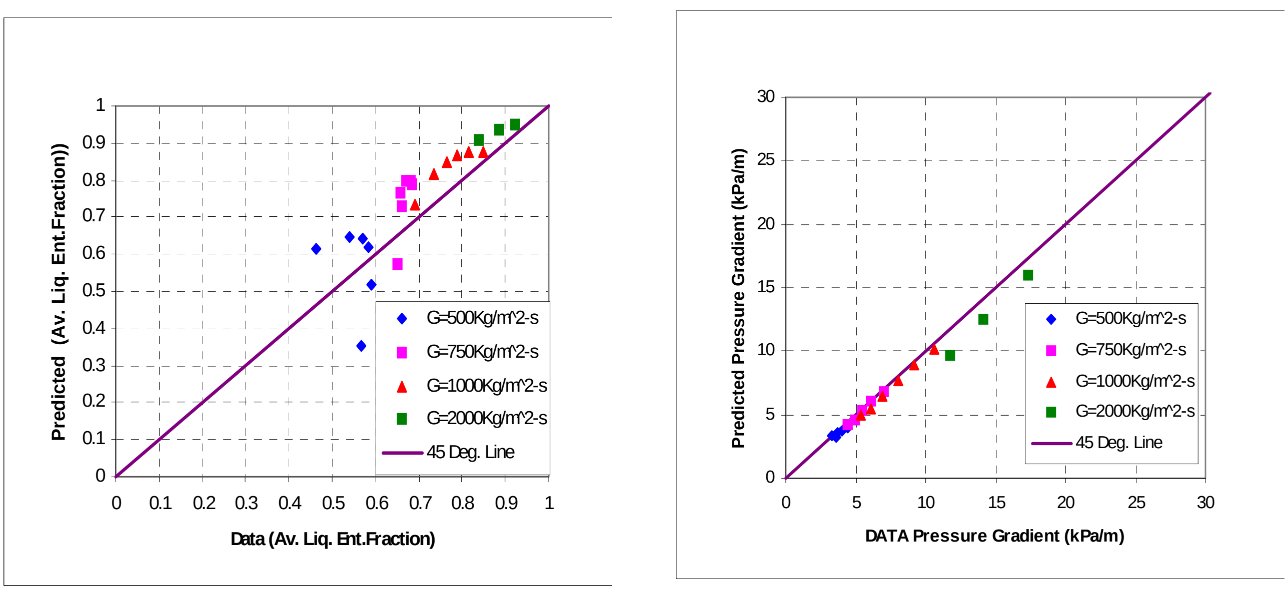

Figure 4 Comparison of COBRAG Prediction with Risø 600 Series Data in 20 mm diameter Round Tube

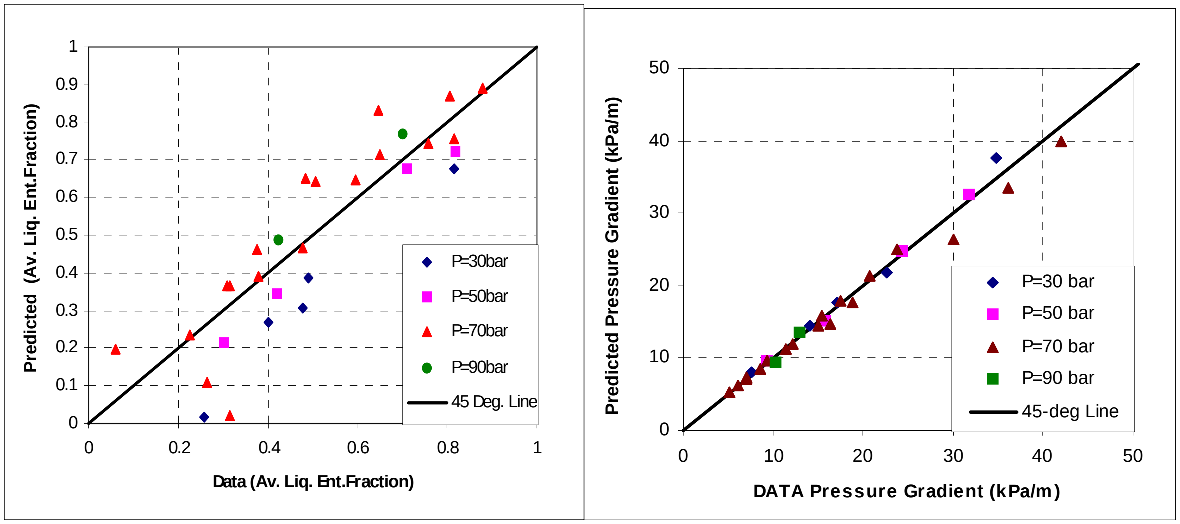

Figure 5 Comparison of COBRAG Prediction with Risø 500 Series Data in 17/26 mm diameter Annulus

The selected combination of entrainment and deposition rate models is:

2.1.1 Entrainment Rate Model

Würtz's liquid entrainment rate model [2] as discussed below is found to be in good combination with the deposition rate model to be discussed in Section 2.1.2.

$$m_e'' = 2.0\left(\frac{\tau_i k_s}{\sigma}\right)\left(\frac{u_g \mu_l}{\sigma}\right) \qquad (\text{kg/m}^2\text{-s}) \qquad (5)$$

The first non-dimensional group in Equation (5) represents a balance between the interfacial shear (τ_i) at the liquid film to vapor interface and the surface tension σ, k_s being the equivalent sand roughness of the film. Würtz [2] recommended the following expression for k_s (in meter)

$$k_s = 0.57\delta + 21.73\times10^3\delta^2 - 38.3\times10^6\delta^3 + 55.68\times10^9\delta^4 \qquad (6)$$

where δ is the average liquid film thickness (in meter). The above expression for equivalent sand roughness, k_s, is valid for δ < 800 micron and may be approximated by $k_s = 6\delta$. This translates to a maximum value of approximately 5 mm, typically one-half of the subchannel hydraulic diameter, for the equivalent sand roughness, k_s. Improved COBRAG calculations discussed in Section 2.2 for a typical heated channel show that at the onset of annular-mist flow, the average liquid film thickness is smaller than 800 micron, and therefore Equation (6) is valid for the annular-mist region of our interest. The average film thickness, δ, is calculated from the three-field conservation equations implemented in COBRAG and the Wallis-type correlation [14] is used for the interfacial shear between the liquid film and the vapor-droplet core flow.

The second non-dimensional parameter in Equation (5) represents a dimensionless vapor velocity that was first suggested by Paleev and Filippovich [15].

2.1.2 Deposition Rate Model

A form similar to Suguwara's droplet deposition correlation [8] including the effect of vapor velocity is found to produce the best results in conjunction with Würtz's entrainment model discussed above. The selected deposition rate is

$$m_d^{''} = au_g \,\mathrm{Re}_g^{-0.2}\, \mathrm{Pr}_g^{-2/3}\, f\left(\frac{1-x_c}{x_c}\right) C \qquad (\mathrm{kg/m^2\text{-}s}) \qquad (7)$$

where x_c is the vapor quality in the vapor-droplet core and 'a' is a GEH proprietary coefficient. This droplet deposition rate model is an improvement over what was used in earlier COBRAG predictions [1].

2.2 Comparison with Risø Heated Tests

Risø heated tests [2] conducted at 70 bar with a central heated 17mm diameter rod inside an unheated 26mm diameter tube were simulated with COBRAG incorporating the selected entrainment and deposition rate models discussed in Section 2.1 above. The length of the heated test section was 3.5 m, typical of the length of a BWR fuel bundle, and subcooled water was introduced at the inlet of the test section. Liquid films from both the inner and outer surfaces of the annulus were extracted at the exit and data on the entrainment fraction were obtained. The mass-flux ranged from 500 to 1000 kg/m^2-s and the exit quality ranged from 0.2 to 0.3. The heated tests simulated here are Run 106, 114 – 116 and 126 [2].

COBRAG (Original) prediction for entrainment fraction (with no other model improvement) was less than satisfactory (see Figure 6). Further investigation revealed that unlike the adiabatic tests discussed in Section 2.1, the lengths of the annular-mist region in these heated tests were small, and the annular-mist flow could not reach an equilibrium or near-equilibrium condition at the exit of the test section. Similar situation is expected in a BWR fuel bundle. Therefore, it is essential that the liquid distribution between the film at the wall and droplets in the vapor core be modelled or initialized correctly at the onset of annular-mist flow regime. This is supported by other investigations [16] in this field. In the improved version of COBRAG, the film flow rate in the pre-annular slug-churn flow regime (transition from a two-field model to a three-field model) is increased such that most of the liquid is in the film increasing its thickness to about twice the earlier value at the onset of annular-mist flow (or three-field model) . The improved entrainment and deposition rate models discussed in Section 2.1 are then applied. This results in a much better prediction of COBRAG (with improved film flow initialization or IFFI) with the measured liquid entrainment fraction at the exit as seen in Figure 6. Similar improvements in the total exit film flow rate predictions are seen in Figure 7. Here two tests (Runs 114 and 116) with the same mass-flux (900 kg/m^2-s) and heat input, but different inlet subcooling, which results in different exit qualities (0.2 for Run 114 and 0.3 for Run 116), are shown. Location of the onset of annular-mist flow regime ranges from approximately 2.7 m (for Run 114) to 1.9 m (for Run 116) from the test section inlet and the maximum average liquid film thickness (for the improved model or IFFI) is approximately 600 micron for both cases. As expected, the film thickness on the heated rod surface is smaller than that on the unheated tube surface. Please note that the film flow rates in the improved COBRAG (IFFI) prediction steadily decrease in the annular-mist region due to liquid evaporation and net entrainment. This trend is in agreement with the experimental data in [16].

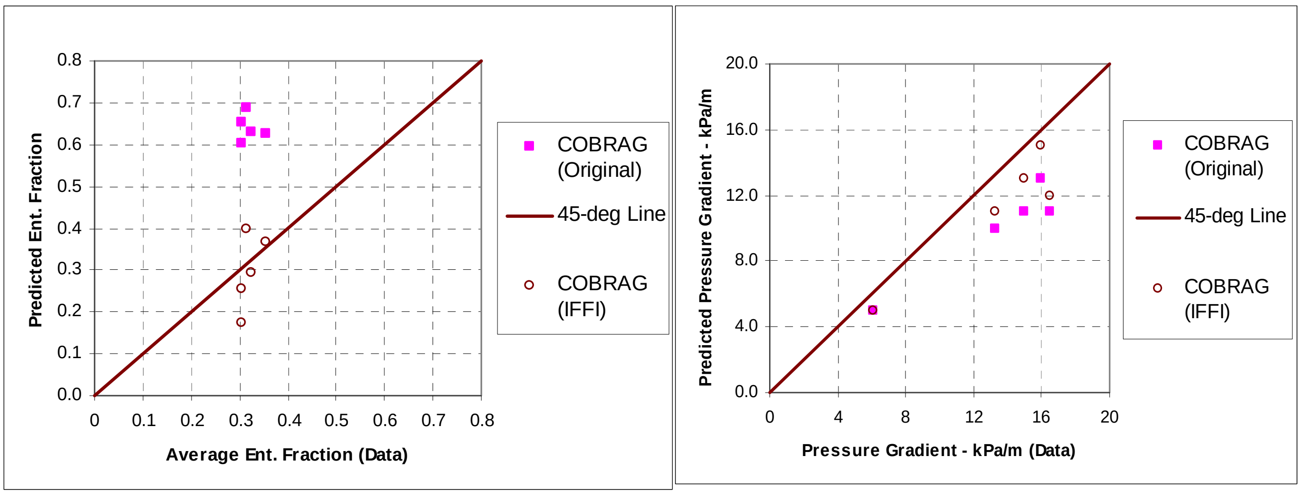

Figure 6 Comparison of COBRAG Prediction with Risø Heated Tests in an Annulus

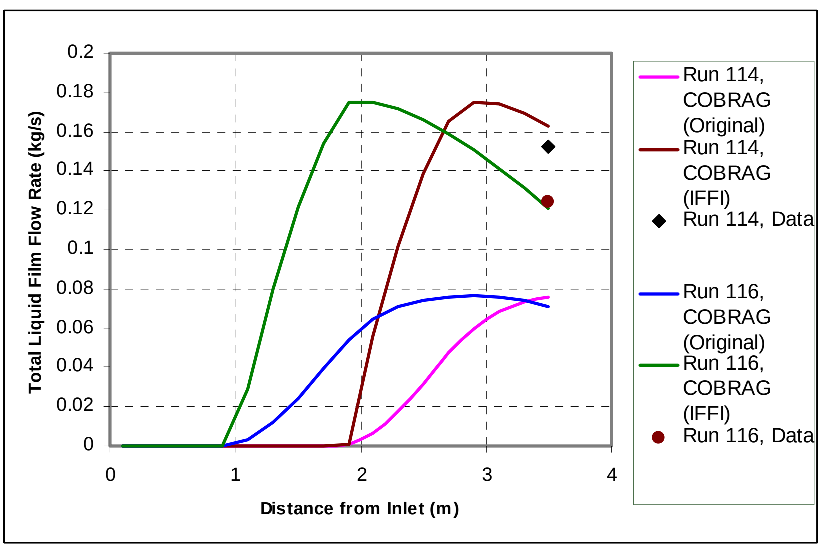

Figure 7 Comparison of COBRAG Prediction of Total Liquid Film Flow Rate with Heated Test Data in an Annulus

3. COBRAG Prediction of Critical Power Tests

As describe in Section 1, the mechanism of BT at BWR condition is due to film dryout. COBRAG multi-field model tracks the liquid film inventory for each rod surface and therefore directly evaluates the onset and location of BT. Physically, the condition for dryout corresponds to the situation where the heating surface is not completely covered by a liquid film. Since surface tension prevents an infinitely thin film, there is a critical film thickness below which the film breaks up to expose the heated surface to the vapor core. Under adiabatic condition, the following model for critical film thickness can be derived by balancing surface tension against interfacial shear at the film surface [17]:

$$\delta_{crit} = \left(\frac{6\sigma}{\rho_\ell} \left(\frac{\mu_\ell}{\tau_i} \right) \right)^{1/3} \tag{8}$$

However disturbance from the core flow tends to destabilize the film by inducing waves on the film surface and results in a larger critical film thickness than that calculated from Equation (8). Refinements to the critical film thickness are usually done based on critical power data. In COBRAG, the critical film thickness is derived based on a large critical power database. The correlation for the critical film thickness depends only on local thermal hydraulic condition, and takes the following functional form with respect to the local mass flux, G:

$$\delta_{crit} = f\left(G\right) \tag{9}$$

Qualification of COBRAG film dryout model for prediction of BT and critical power is carried out using GE experimental data for vertical up-flow in an annulus under wide range of test conditions [18], and for full-scale prototypic critical power tests conducted in an 8x8-rod bundle including spacers. More rod bundle tests are being included in the COBRAG qualification matrix.

The critical film thickness (Equation 9) used in the improved COBRAG is on the order of 10 micron. Since the vapor-droplet core velocity significantly affects wave generation on the liquid film, the critical film thickness is an ascending function of the local mass flux, G. Some researchers [19] prefer to use zero film thickness or zero film flow rate as the criterion for dryout. However, the present authors feel that a physics-based critical film thickness correlation such as Equation (9) above can better capture the reality of film break-up or dry patch formation at the onset of boiling transition (BT).

3.1 GE Single Rod Test in an Annulus

High-pressure (70 bar) steam-water critical power tests conducted with a heated rod inside an unheated tube or annulus [18] provided good data to qualify the critical film thickness model along with the entrainment and deposition rate models discussed earlier. Several different test sections were used in [18]. The tests simulated here were conducted with a 13.7 mm I.D. heater rod inserted in a 22.2 mm O.D. annulus. The length of the test section was 2.74 m. Subcooled water was introduce at the inlet and uniform heating was applied until dryout or critical power condition was observed at the test section exit. The mass-flux ranged from 400 to 2000 kg/m^2-s and only the data with exit quality greater than 20% are considered here to ensure annular or annular-mist regime at the exit or dryout location.

Figure 8 shows good comparison between the predicted critical power by COBRAG and the experimental data. Combination of improved entrainment and deposition rate models, improved liquid distribution in the film at the onset of annular or annular-mist flow, and the critical film thickness model discussed above results in good prediction over the wide range of mass-flux and exit quality. It is worth noting that the COBRAG results presented in Figure 8 are obtained without considering any spacer effect since the blockage or obstruction due to the 'retaining' pins was minimal.

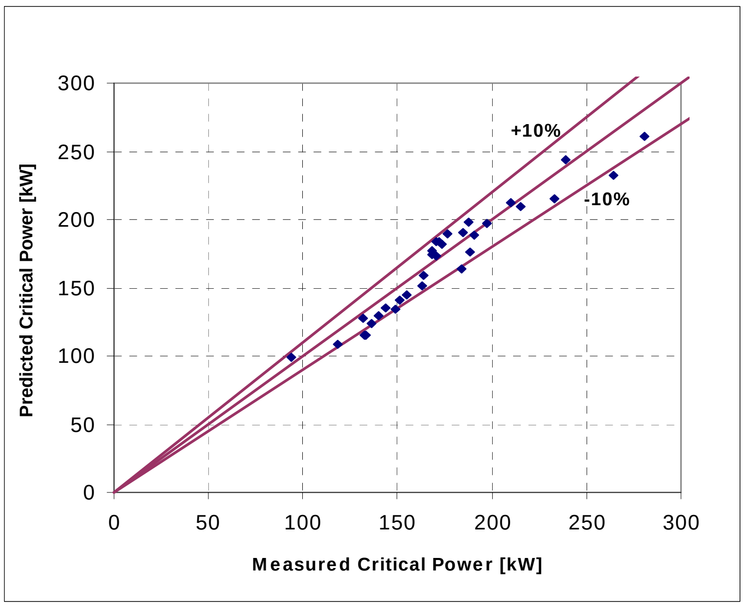

Figure 8 COBRAG Critical Power Predictions for GE Single Rod Test Data

3.2 GE Bundle Tests

GE proprietary critical power tests conducted in an 8x8 rod bundle with 'Ferrule' grid spacers were simulated by the improved COBRAG. The test pressure was 70 bar, the mass-flux ranged from 300 to 2000 kg/m^2-s, and the inlet subcooling ranged from 10 to 60 K. Two types of axial power shapes, namely chopped cosine and inlet peaked were used. Figure 9 shows the comparison between the COBRAG predictions and the test data for both critical power and bundle pressure drop. Please note that the tests for critical power and pressure drop were different, but the improved COBRAG predicts both sets of data within ±10%. Location of boiling transition (BT), both radial (or rod-wise) and axial, was also reasonably well-predicted.

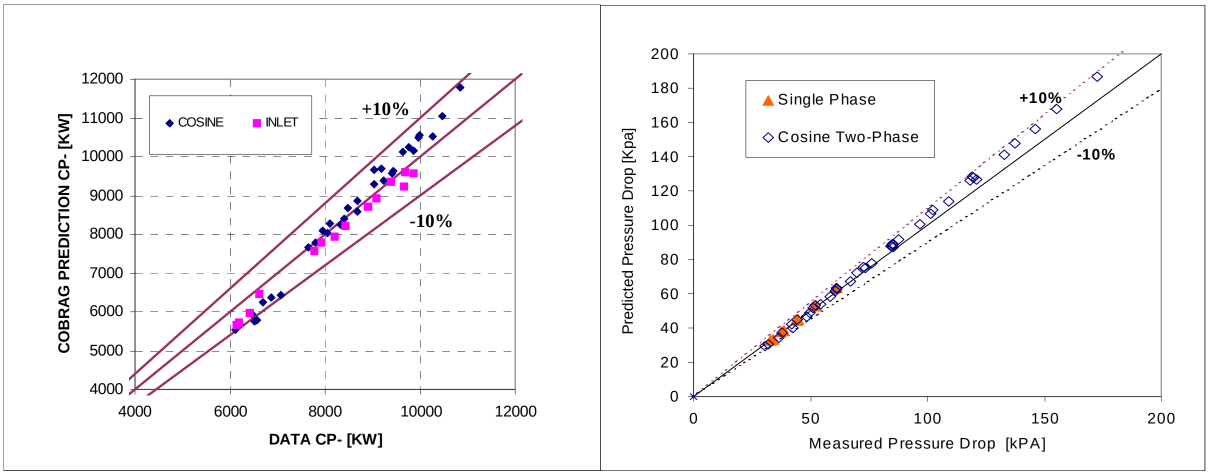

Figure 9 COBRAG Critical Power and Pressure Drop Predictions for GE 8x8 Rod Bundle Test Data

It is worth noting that a few spacer-specific input parameters for the GE 8x8 ferrule spacer had to be used since developing a spacer model from first principles is very difficult, if not impossible [20]. These inputs are related to the specific geometry of the spacer hardware, cross-sectional flow area blocked by the spacer hardware, turbulence enhancement that increases droplet re-deposition, etc. The same inputs are applied for all flow conditions and axial power shapes for the same spacer. Different spacers are expected to require some adjustments to these spacer-specific inputs.

4. Summary and Conclusions

Predictions of the COBRAG code, based on a three-fluid multi-film model, have been systematically compared with the measurements of film flow rate and liquid entrainment fraction under adiabatic and diabatic conditions in simple geometries such as round tubes and annulus. Based on these comparisons, the models for entrainment and deposition rates and the initial liquid distribution between the film and the droplets in the vapor core at the onset of annular-mist flow regime for heated tests have been improved. The code with these improvements was then applied to the critical power tests conducted in an annulus and an 8x8 rod bundle with two different axial power shapes. Good agreement with the critical power and pressure drop data and the systematic approach undertaken in this study provide confidence in the predictive capability of the COBRAG film dryout and associated models.

5. References

[1] B. Hizoum, J. Andersen, A. Sakouda and S. Bowman, “COBRAG Subchannel Analysis of BWR Fuel Thermal Hydraulic Performance”, Proceedings of 2010 LWR Fuel Performance/ TopFuel/WRFPM, Paper 90, Orlando, Florida, USA, September 26-29, 2010, pp. 668-680.

[2] J. Würtz, "An Experimental and Theoretical Investigation of Annular Steam-Water Flow in Tubes and Annuli at 30 to 90 bar", Risø National Laboratory Report No. 372, Denmark, April 1978.

[3] R. T. Lahey, Jr. and F. J. Moody, "The Thermal-Hydraulics of a Boiling Water Nuclear Reactor", Second Edition, Section 4.4, American Nuclear Society, La Grange Park, Illinois, USA, 1993.

[4] G. F. Hewitt and N. S. Hall-Taylor, "Annular Two-Phase Flow", Pargamon Press, New York, USA, 1970.

[5] G. F. Hewitt and P. B. Whalley, "Vertical Annular Two Phase Flow", Multiphase Science and Technology, Vol. 4, Chapter 2, Edited by G. F. Hewitt, J. M. Delhaye and N. Zuber, Hemishere Publishing Corporation, New York, USA, 1989.

[6] T. Okawa, A. Kotani and I. Kataoka, "Experiments for liquid phase mass transfer rate in annular regime for a small vertical tube", *Int. Journal of Heat and Mass Transfer*, Vol. 48, 2005, pp. 585-598.

[7] P. B. Whalley, "Boiling, Condensation, and Gas-Liquid Flow", Chapter 9, Clarendon Press, Oxford, UK, 1987.

[8] S. Sugawara, "Droplet Deposition and Entrainment Modeling based on the Three-Fluid Model," Proceedings of 3rd Int. Topical Meeting on Nuclear Power Plant Thermal Hydraulics and Operations, Seoul, Korea, November 1988, pp. A1-19-A1-28.

[9] T. Okawa, T. Kitahara, K. Yoshida, T. Matsumoto and I. Kataoka, "New entrainment rate correlation in annular two-phase flow applicable to wide range of flow condition", Int. Journal of Heat and Mass Transfer, Vol. 45, 2002, pp. 87-98.

[10] G. F. Hewitt, "Correlations for Deposition and Entrainment Rates", Section 2.2.4.4 in Handbook of Multiphase Systems, Editor-in-Chief G. Hetsroni, Hemishere Publishing Corporation, Washington, USA, 1982.

[11] G. F. Hewitt and A. H. Govan, "Phenomenological modelling of non-equilibrium flows with phase change", *Int. Journal of Heat and Mass Transfer*, Vol. 33, 1990, pp. 229-242.

[12] T. Okawa, T. Kitahara, K. Yoshida, T. Matsumoto and I. Kataoka, "A simple correlation of droplet entrainment in annular-dispersed two-phase flows", Proceedings of 4th Int. Conference on Multiphase Flow, Paper No. 396, New Orleans, USA, May 27-June 1, 2001.

[13] T. Okawa and I. Kataoka, "Correlations for the mass transfer rate of droplets in vertical upward annular flow", *Int. Journal of Heat and Mass Transfer*, Vol. 48, 2005, pp. 4766-4778.

[14] G. B. Wallis, "One-dimensional Two-phase Flow", Chapter 11, McGraw-Hill Book Company, New York, USA, 1969.

[15] I. I. Paleev and B. S. Filippovich, “Phenomena of liquid transfer in two-phase dispersed annular flow”, *Int. Journal of Heat and Mass Transfer*, Vol. 9, 1966, pp. 1089-1093.

[16] C. Adamsson and H. Anglart, “Film flow measurements for high-pressure diabatic annular flow in tubes with various axial power distributions”, *Nuclear Engineering and Design*, Vol. 236, 2006, pp. 2485-2493.

[17] B. S. Shiralkar and K. H. Chu, “Recent Trends in Subchannel Analysis,” Subchannel Analysis in Nuclear Reactor, Edited by H. Ninokata and M. Aritomi, The Institute of Applied Energy and Atomic Energy Society of Japan, 1992.

[18] E. Janssen and J.A. Kervinen, “Burnout Conditions for Single Rod in Annular Geometry, Water at 600 to 1400 psia”, GEAP-3899, February 1963.

[19] C. Adamsson and J-M. Le Corre, “Modeling and validation of a mechanistic tool (MEFISTO) for the prediction of critical power in BWR fuel assemblies”, *Nuclear Engineering and Design*, 2011, in press.

[20] K. H. Chu and B. S. Shiralkar, “Study of Spacer Effect on Critical Power by COBRAG Based on a Two-Fluid and Multi-Field Model”, Paper 14, Proceedings of Second International Seminar on Subchannel Analysis, EPRI TR-103188s, Palo Alto, CA, USA, November 1993.

Copyright